

STUDY ON AERODYNAMIC VIBRATIONS OF A BRACING MEMBER WITH A RECTANGULAR CROSS SECTION OF A LONG-SPANDED TRUSS BRIDGE

Kentaro Suda⁺¹, Kazutoshi Matsuda⁺¹, Kusuo Kato⁺¹ and Yusuke Tamai⁺²
⁺¹ Kyushu Institute of Technology, Kitakyushu, Japan
⁺² Hitachi, Ltd., Tokyo, Japan

In 2009, Ikitsuki Bridge, a truss bridge in Nagasaki Prefecture with a center span length of 400 m, was discovered to have a crack in the bracing member of the bridge. As a result of the subsequent vibration measurement at the site, the main cause of the crack was identified as Kármán vortex-induced excitation. However, vibrations were also observed in the wind speed range of 7-8 m/s, which was lower than the resonance wind speed of Kármán vortex-induced excitation. Conventionally, according to the results from a wind tunnel test using a side ratio of $B/D=2-8$ (B: along-wind length, D: cross-wind length), the motion-induced vortex excitation was confirmed. However, the side ratio of the section of the bracing member is $B/D=1.18$, and the motion-induced vortex excitation in the case of this side ratio has not yet to be confirmed by the conventional wind tunnel test. Therefore, in this research, a spring-supported test was carried out targeting a rectangular cross section of $B/D=1.18$. Furthermore, flow visualization was performed and the results of the spring-supported test were discussed. The vibrations in the bracing member with a rectangular cross section ($B/D=1.18$) of Ikitsuki Bridge generated in the wind speed range of lower than Kármán vortex-induced excitation among the aerodynamic vibrations caused by wind were suggested to possibly be motion-induced vortex excitation by experimental results of a spring-supported test and the flow visualization. Further investigation should be undertaken.

Keyword: bracing member, rectangular cross section, motion-induced vortex excitation, Kármán vortex-induced excitation, spring supported test, flow visualization

1. INTRODUCTION

The vortices separated from rectangular cross sections are broadly classified into Kármán vortices and motion-induced vortices (vortices separated from leading edge)^{1, 2)}. The former are those that are accompanied by the interferences of two separated shear layers at both the top and bottom surfaces of the structures. The latter are the ones that are shedding separately from the leading edges of the top and bottom surfaces caused by the separated shear layers at the top and bottom surfaces excited alternately due to the vibration of the rectangular cross section. The vibration caused by the latter vortices was found in the past wind tunnel tests^{3, 4)}. The vibration is known as either motion-induced vortex excitation^{1, 2)} or impinging-shear-layer instability⁵⁻⁸⁾. The onset wind speed of this vibration depends on the side ratio of the rectangular cross section and this relationship is schematically clarified^{1), 8)}. The mechanisms of the motion-induced vortex excitation of the rectangular section and H-shaped section cylinders are also revealed⁹⁻¹²⁾. This research is involved in the motion-induced vortex excitation and Kármán vortex-induced excitation generated in a bracing member of a real truss bridge in Japan.

In 2009, Ikitsuki Bridge, a truss bridge in Nagasaki Prefecture with a center span length of 400 m, was discovered to have a crack in the bracing member of the bridge¹³⁾. As a result of the subsequent vibration measurement at the site, the main cause of the crack was identified as Kármán vortex-induced excitation. However, vibrations were also observed in the wind speed range of 7-8 m/s, which was lower than the resonance wind speed of Kármán vortex-induced excitation. Conventionally, according to the results from a wind tunnel

test using a side ratio of $B/D=2-8$, the motion-induced vortex excitation was confirmed¹⁾. However, the side ratio of the section of the bracing member is $B/D=1.18$, and the motion-induced vortex excitation in the case of this side ratio has not yet to be confirmed by the conventional wind tunnel test. Therefore, in this research, a spring-supported test was carried out targeting a rectangular cross section of $B/D=1.18$. Furthermore, flow visualization was performed and the results of the spring-supported test were discussed. In order to clarify the relationship between the generation of motion-induced vortices and the side ratio of B/D , flow visualization was conducted by changing a side ratio of B/D from 0.5 to 1.5.

2. EXPERIMENTAL SETUPS

(1) Section models

Table 1 shows the scale and dimensional data of the section model, $B/D=1.18$, used in each test. Two cross-sections of a rectangular cross-section and a cross-section with a flange, a reproduction of the cross-section of the cracked bracing member of Ikitsuki Bridge, were used. Table 2 shows the dimensional data of the models used for the flow visualization test. The models used for the flow visualization tests were rectangular section models without flanges, because the spring-supported test results were not influenced by the existence or non-existence of flanges when an angle of attack was 0 degrees. The reason for this will be described later. Table 3 shows the dimensional data of the models used for the 2nd spring-supported tests.

Table 1: Section models ($B/D=1.18$)

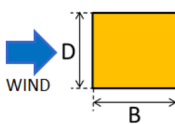
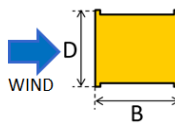
Wind tunnel tests	Model scale				
		B(mm)	D(mm)	B(mm)	D(mm)
1 st spring-supported tests	1/5.6	107	90.0	107	90.0
Flow visualization	1/12.5	47.2	40.0		

Table 2: Section models for flow visualization

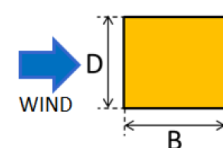
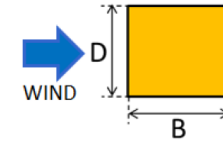
Cross-section	B/D	B(mm)	D(mm)
	2.0	80.0	40.0
	1.5	60.0	
	1.18	47.2	
	1.0	40.0	
	0.75	30.0	
	0.62	24.8	
	0.50	20.0	

Table 3: Section models for 2nd spring-supported tests

Cross-section	B/D	B(mm)	D(mm)
	1.18	212.4	180.0
	1.0	180.0	
	0.75	135.0	
	0.62	111.6	
	0.50	90.0	

(2) 1st spring-supported tests

The spring-supported test for $B/D=1.18$ was conducted in the closed circuit wind tunnel (cross-section: 1.8m high \times 0.9m wide) at Kyushu Institute of Technology. Main experimental conditions for the model were: mass per unit length=3.12 kg/m, natural frequency of heaving vibration=9.13 Hz, logarithmic decrement of structural damping=0.0021 and Scruton number=1.32. Table 4 shows the conditions for the spring-supported test. Figure 1 shows a photo of the section model installed in the wind tunnel.

Table 4: 1st spring-supported test conditions for $B/D=1.18$

Angle of attack, α	0, 10 deg.
Yaw angle, β	0 deg.
Mass per unit length, m	3.12 kg/m
Natural frequency, f	9.13Hz
Structural damping (in logarithmic decrement), δ	0.0021
Scruton number, $Sc=2m\delta/\rho D^2$	1.32
Blockage ratio	5 %

ρ : air density=1.23kg/m³, D: model height =0.090m, L: Model length=0.76m



Figure 1: Section model for spring-supported tests mounted in Kyushu Institute Technology wind tunnel

(3) Flow visualization

The flow visualizations around the model during static and oscillating times were conducted using a small-sized wind tunnel (0.4m high \times 0.4m wide) at Kyushu Institute of Technology. It was considered that the wind speeds in the wind tunnel of $V=0.6$ -1.0 m/s are good for visualization, so that eventually $V=0.6$ m/s and 1.0 m/s were selected at the onset wind speeds of motion-induced vortex excitation and Kármán vortex-induced excitation, respectively. Accordingly, the experimental Reynolds numbers are $Re=VD/\nu=1.6\times 10^3$ and 2.7×10^3 , respectively. As for the forced-oscillating amplitude η , because the peak of aerodynamic response in the range of low wind speed is $2\eta/D=0.12$, the non-dimensional double amplitudes were set up as $2\eta/D=0.10$, 0.05 and 0.025 in accordance with the spring-supported test results. Tables 5 and 6 show the conditions for the flow visualization tests.

Table 5: Flow visualization test conditions at the onset wind speed of motion-induced vortex excitation

B/D	B (mm)	D (mm)	Angle of attack α (deg.)	Reduced wind speed $V_r=V/fD$ ($=1.67B/D$) ¹⁾	Wind speed V(m/s)	Frequency of forced oscillation method f(Hz)
0.50	20.0	40	0	0.8	0.6	18.0
0.62	24.8			1.0		14.5
0.75	30.0			1.3		12.0
1.00	40.0			1.7		9.0
1.18	47.2			2.0		7.6
1.5	60.0			2.5		6.0
2.0	80.0			3.3		4.5

Table 6: Flow visualization test conditions at the onset wind speed of Kármán vortex-induced excitation

B/D	B (mm)	D (mm)	Angle of attack α (deg.)	Strouhal number $St=fD/V$	$V_r=V/fD$ ($=1/St$)	Wind speed V(m/s)	Frequency of forced oscillation method f(Hz)
1.18	47.2	40	0	0.122	8.20	1.0	3.0

(4) 2nd spring-supported tests

Spring-supported tests were conducted on $B/D=0.5-1.18$ based on the results of the flow-visualization experiment. Table 7 shows the 2nd spring-supported test conditions for $B/D=1.18$. Because the cross-sectional side ratio, which was the object of the experiment, was smaller than that of the first spring-supported test, the measured reduced wind-speed range was very low. Therefore, in order to lower the natural frequency of the vibration system to a value which can be experimented, the size of the cross section of the model had to be enlarged. Due to experimental restrictions such as this, the blockage ratio was changed to 10%. Because the blockage ratio in the first spring-supported tests was 5%, it was confirmed at the beginning that, in the case of $B/D=1.18$, the difference in blockage ratio did not influence the response characteristics.

Table 7: 2nd spring-supported test conditions for $B/D=1.18$

Angle of attack, α	0 deg.
Yaw angle, β	0 deg.
Mass per unit length, m	3.76 kg/m
Natural frequency, f	5.70Hz
Structural damping (in logarithmic decrement), δ	0.0085
Scruton number, $Sc=2m\delta/\rho D^2$	1.64
Blockage ratio	10 %

ρ : air density=1.20kg/m³, D: model height =0.180m, L: Model length=0.828m

3. EXPERIMENTAL RESULTS AND DISCUSSION

(1) 1st spring-supported tests

Figure 2 shows the result of the spring-supported test for an angle of attack of 0 degrees¹⁴⁾. Vibrations were confirmed from the neighborhoods of reduced wind speed $V_r=2$ and 8. Because the reduced wind speed at motion-induced vortex excitation is calculated as $V_r=1.67 \times B/D=1.67 \times 1.18=2.0^1)$, vibrations around $V_r=2$ were considered to be motion-induced vortex excitation. The effects of the existence or non-existence of flange on the maximum response amplitude of motion-induced vortex excitation are extremely small. However, Figure 3 shows the result of an experiment separately conducted for an angle of attack of 10 degrees that the maximum response amplitude in the case with flanges was approximately 1.5 times larger than that in the case with no flange. In other words, it turns out that as the angle of attack becomes larger, the existence or non-existence of flange tends to exercise an effect on the patterns of the flows around the cross-section.

The Strouhal number measured on the cross-section with flanges was $St=0.124$. Its inverse number is the critical reduced wind speed of beginning Kármán vortex-induced excitation. In other words, because $V_r=1/St=8.1$, a vibration beginning in the neighborhood of a reduced wind speed of 8 can be judged as Kármán vortex-induced excitation. However, from the fact that the Scruton number in this experiment's case was small at $Sc=1.32$, it was found that Kármán vortex-induced excitation was changed to a galloping along with the increase in wind speed.

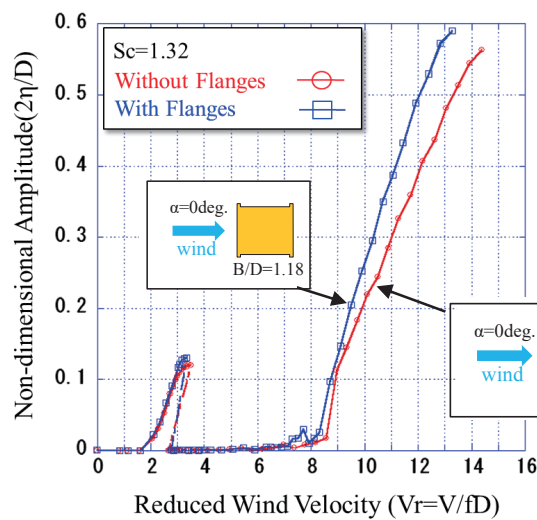


Figure 2: Spring-supported test result (Angle of attack, $\alpha=0$ deg., Yaw angle, $\beta=0$ deg.)¹⁴⁾

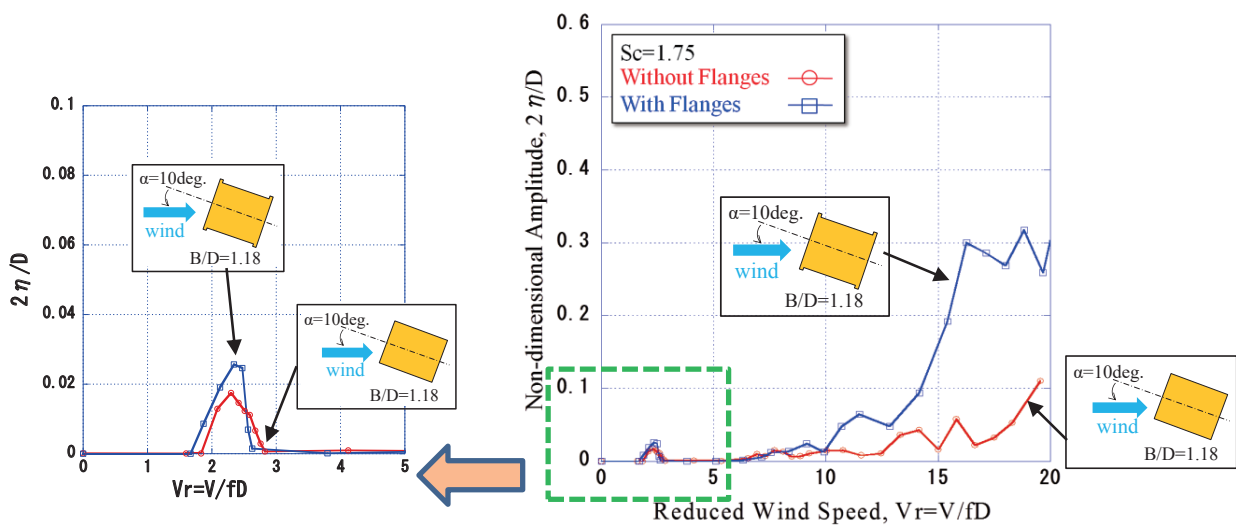


Figure 3: Spring-supported test result (Angle of attack, $\alpha=10$ deg., Yaw angle, $\beta=0$ deg.)¹⁴⁾

(2) Flow visualization

a) B/D=1.18 cross-section of the bracing member of Ikitsuki Bridge

From the response characteristics of Figures 2 and 3, the possibility of the existence of motion-induced vortex excitation at the neighborhood of $V_r=2$ was suggested. The possibility of the existence of motion-induced vortex excitation of $B/D=1.18$ was discussed here from the aspects of the flow visualization.

Table 8 shows the results of the flow visualization of the cross-section of $B/D=1.18$. At static time, only Kármán vortices were formed in the same way as in the case of the experiment at $B/D=2.0$. At the time of oscillation at the onset wind speed of motion-induced vortex excitation, although separated vortices from leading edge were formed, no secondary vortices at trailing edge were formed. Due to the fact that secondary vortices at trailing edge were confirmed at the cross-section of $B/D=2.0$ at the time of oscillation as shown in Figure 4(a) which was carried out to confirm the validity of the experimental method of the research, it was suggested that when the side ratio of B/D becomes small, secondary vortices at trailing edge tend not to be formed.

The generation of motion-induced vortex excitation is considered to be caused by the unification of separated vortices from leading edge and secondary vortices at trailing edge¹⁾. However, according to the spring-supported test results targeting $B/D=1.18$ where the formation of secondary vortices at trailing edge were not observed, aerodynamic vibrations considered to be motion-induced vortex excitation were confirmed as shown in Figures 2 and 3. Although it was suggested that motion-induced vortex excitation would possibly occur at the range of low wind speed even in the case of side ratios where secondary vortices at trailing edge were not confirmed, further investigation should be undertaken to confirm.

Table 8: Results of flow visualization ($B/D=1.18$, Angle of attack, $\alpha=0$ deg.)

	<p style="text-align: center;">$2\eta/D$</p> <p style="text-align: center;">V_r</p> <p style="text-align: center;">(Re=$VD/v=1.6 \times 10^3$)</p>	<p style="text-align: center;">$2\eta/D$</p> <p style="text-align: center;">V_r</p> <p style="text-align: center;">(Re=$VD/v=2.7 \times 10^3$)</p>
Fixed model		
Forced-oscillating model at the top displacement ($2\eta/D=0.10$)		

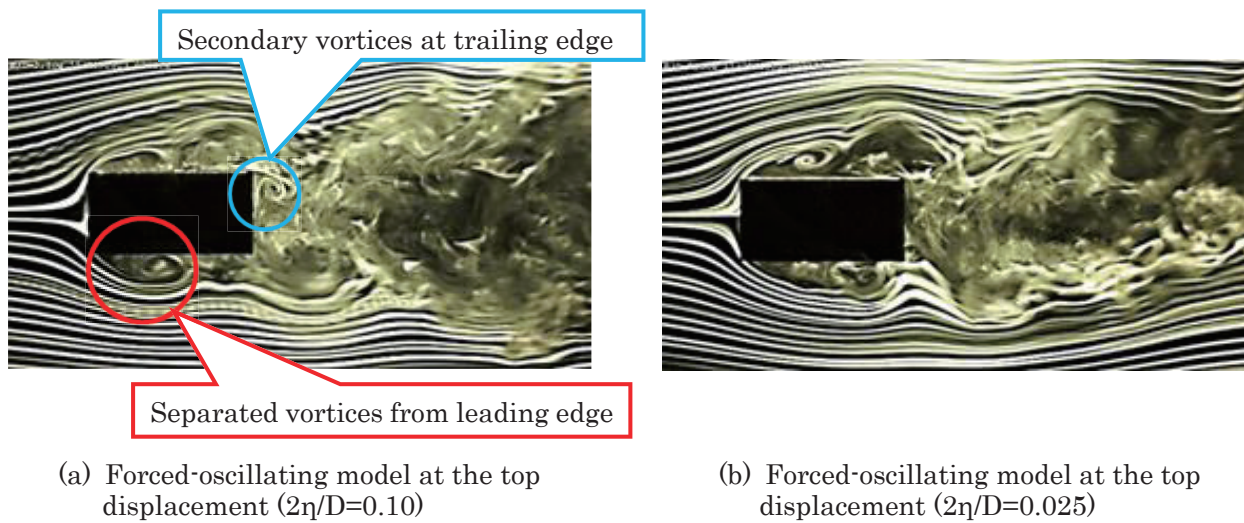


Figure 4: Flow visualization (Validity of experimental method, $B/D=2.0$, Angle of attack, $\alpha=0$ deg., $V_r=3.3$)

b) Rectangular cross-sections of less than $B/D=1.5$

For the purpose of clarifying the relationship between the formations of separated vortices from leading edge and the side ratio of B/D , the flow visualizations around the cross-section were conducted by the side ratio being changed from 0.5 to 1.5. Table 9 shows the experimental results of the flow visualization at the side ratio of $B/D=0.5-1.5$. In the experimental results of non-dimensional double amplitude $2\eta/D=0.050$, the generation of separated vortices from leading edge were confirmed in all B/D s. However, as a result of non-dimensional double amplitude $2\eta/D=0.025$, the vortices that separated from the leading edge were gradually separating from the top and bottom surfaces of the cross-sections of less than $B/D=0.62$ and flowing downward. The generation of secondary vortices at trailing edge was not confirmed clearly in all cross-sections of less than $B/D=1.5$.

(3) 2nd spring-supported tests

Table 10 shows the results of the spring supported test. Motion-induced vortex excitation was confirmed in the three cross sections of $B/D=1.18$, 1.0 and 0.75. The less the side ratio B/D is, the less the maximum amplitude of motion-induced vortex excitation tends to become. It is considered that if the side ratio B/D becomes smaller, the areas of the upper and lower surfaces of the model, on which fluctuating lift acts, gradually reduce and as a result, exciting force becomes smaller. The reason why motion-induced vortex excitation did not generate in $B/D=0.62$ and 0.5 for $Sc=1.6$, it is presumed, is that the separated vortex from the leading edge gradually separate from the upper and lower surfaces of the model and flow down as shown in Table 9, and therefore, fluctuating lift does not fully act on the upper and lower surfaces of the model. However, motion-induced vortex excitation was confirmed in $B/D=0.62$ for $Sc=0.82$.

Then, it turns out that there is a difference between the estimated critical wind speed of Kármán vortex-induced excitation $1/St$ calculated from the inverse number of the measured Strouhal number St and the experimental critical wind speed of Kármán vortex-induced excitation in $B/D=0.62$ and 0.5. As Hirata¹⁷⁾ pointed out, the vibration of the reduced wind speed generated in the neighborhood of 4 is considered to be a low speed galloping in the cases of $B/D=0.62$ and 0.5.

Table 9: Results of flow visualization around forced-oscillating rectangular section models at the top displacement at the onset wind speed of motion-induced vortex excitation (Angle of attack, $\alpha=0$ deg.)

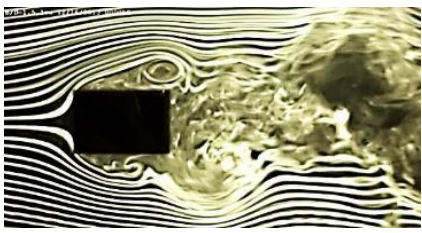
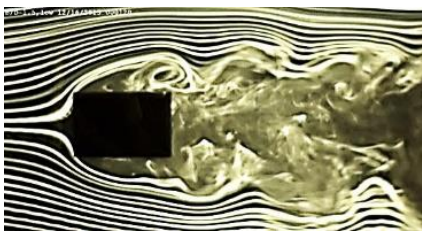
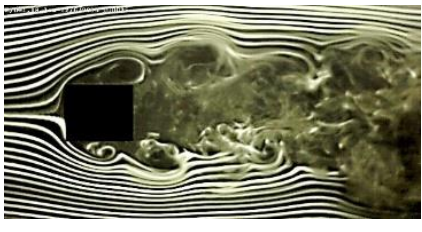
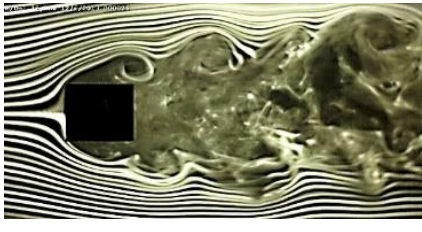


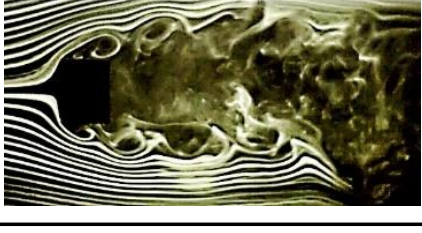
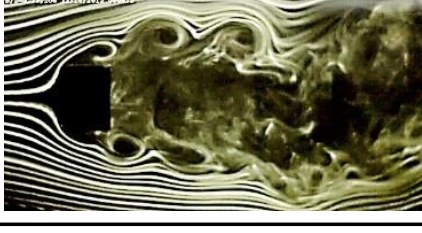
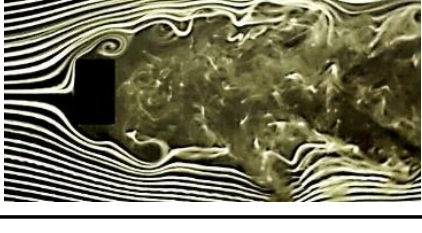
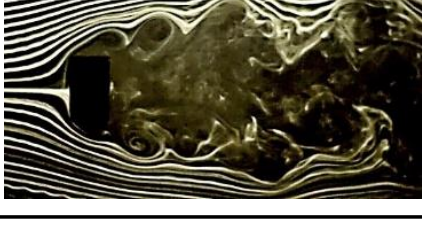
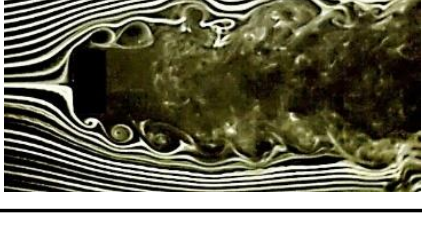
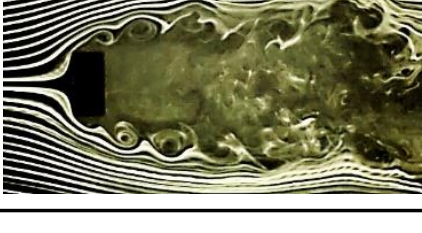
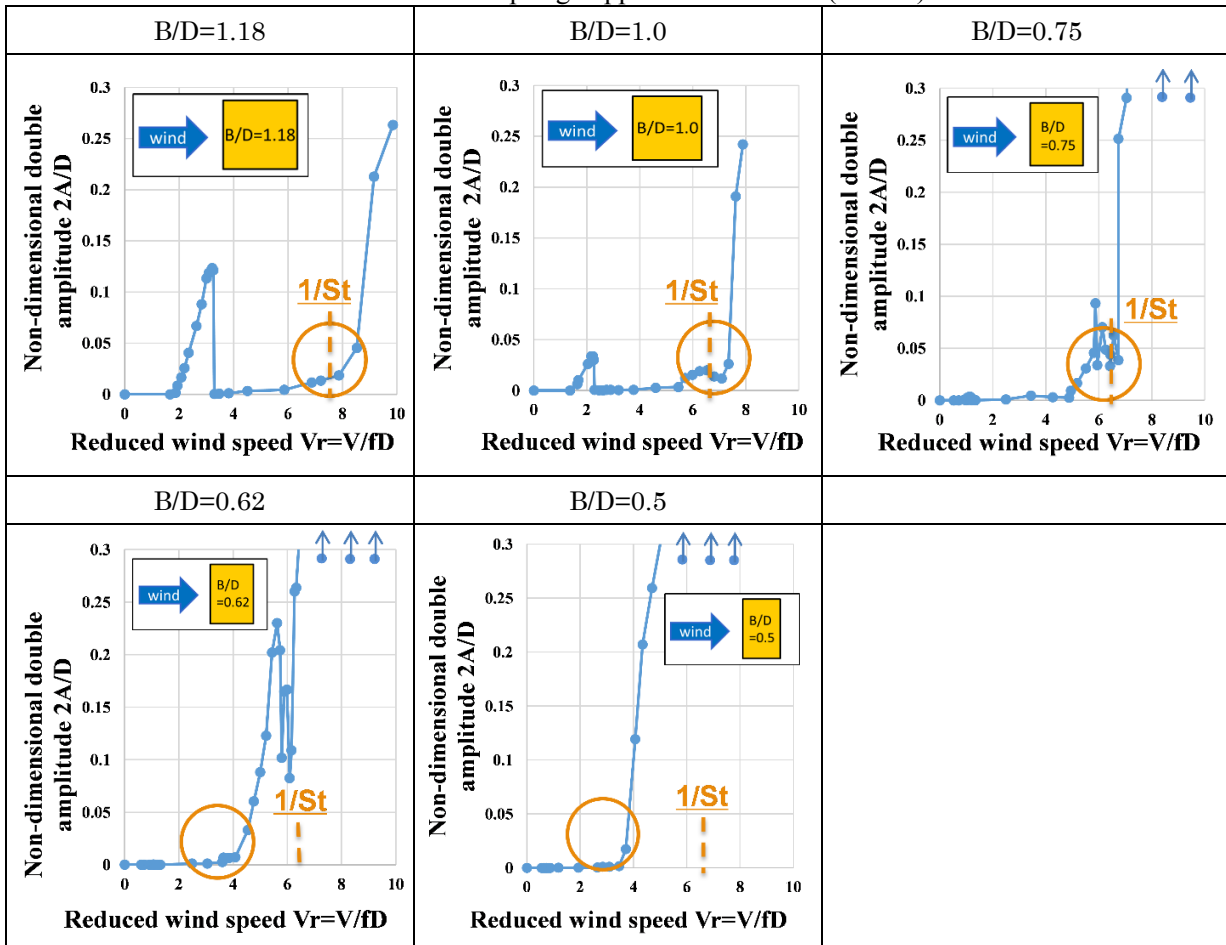
B/D	Vr	$2\eta/D = 0.050$	$2\eta/D = 0.025$
1.50	2.5		
1.18	2.0		
1.0	1.7		
0.75	1.3		
0.62	1.0		
0.50	0.8		

Table 10: 2nd spring-supported test results ($Sc=1.6$)

4. CONCLUSIONS

The findings obtained from this research are as follows:

- (1) The vibrations of the bracing member with a rectangular cross section ($B/D=1.18$) of Ikitsuki Bridge generated in the wind speed range of lower than Kármán vortex-induced excitation among the aerodynamic vibrations caused by wind were suggested to possibly be motion-induced vortex excitation by experimental results of the spring-supported test and the flow visualization test. Further investigation should be undertaken.
- (2) Given that this aerodynamic vibration is motion-induced vortex excitation, the possibility was suggested that motion-induced vortex excitation might be generated even at side ratios of less than $B/D=2.0$ where the generation of secondary vortices at trailing edge was not confirmed.
- (3) Aerodynamic vibration which can be considered to be motion-induced vortex excitation was also confirmed in the three cross sections of $B/D=1.18$, 1.0 and 0.75 . The less the side ratio B/D is, the less the maximum response amplitude of motion-induced vortex excitation tends to become. The reason why motion-induced vortex excitation did not generate in $B/D=0.62$ and 0.5 for $Sc=1.6$, it is presumed, is that the separated vortices from the leading edge gradually separate from the upper and lower surfaces of the model and flow down, and therefore, fluctuating lift does not fully act on the upper and lower surfaces of the model. However, motion-induced vortex excitation was confirmed in $B/D=0.62$ for $Sc=0.82$.

REFERENCES

- 1) N. Shiraishi, M. Matsumoto: On classification of vortex-induced oscillation and its application for bridge structures, *Journal of Wind Engineering and Industrial Aerodynamics*, Vol.14, Nos.1-3, pp.419-430, 1983.
- 2) S. Komatsu and H. Kobayashi: Vortex-induced oscillation of bluff cylinders, *Journal of Wind Engineering and Industrial Aerodynamics*, Vol.6, pp.335-362, 1980.
- 3) M. Novak: Galloping and vortex induced oscillations of structures, *Proceedings of the Third International Conference on Wind Effects on Buildings and Structures*, Tokyo, Japan, pp.799-809, 1971.
- 4) Y. Otsuki, K. Washizu, H. Tomizawa, A. Ohya and K. Fujii: Experiments on the aeroelastic instability of prismatic bars with rectangular sections, *Proceedings of the Third International Conference on Wind Effects on Buildings and Structures*, Tokyo, Japan, pp.891-898, 1971.
- 5) D. Rockwell and E. Naudascher: Review- Self-sustaining oscillations of flow past cavities, *Transactions of the ASME, Journal of Fluids Engineering*, Vol.100, pp.152-165, 1978.
- 6) Y. Nakamura, Y. Ohya and H. Tsuruta: Experiments on vortex shedding from flat plates with square leading and trailing edge, *Journal of Fluid Mechanics*, Vol. 222, pp.437-447, 1991.
- 7) Y. Ohya, Y. Nakamura, S. Ozono, H. Tsuruta and R. Nakayama: A numerical study of vortex shedding from flat plates with square leading and trailing edges, *Journal of Fluid Mechanics*, Vol. 236, pp.445-460, 1992.
- 8) E. Naudascher and Y. Wang: Flow-induced vibrations of prismatic bodies and grids of prisms, *Journal of Fluids and Structures*, Vol.7, pp.341-373, 1993.
- 9) M. Matsumoto, N. Shiraishi, H. Shirato, S. Stoyanoff, and T. Yagi: Mechanism of, and turbulence effect on vortex-induced oscillations for bridge box girders, *Journal of Wind Engineering and Industrial Aerodynamics*, Vol. 49, Issues 1-3, pp.467-476, 1993.
- 10) Y. Kubo, K. Hirata and K. Mikawa: Mechanism of aerodynamic vibrations of shallow bridge girder sections, *Journal of Wind Engineering and Industrial Aerodynamics*, Vol.41-44, pp.1297-1308, 1992.
- 11) R. Mills, J. Sheridan, K. Hourigan and M.C. Welsh: The mechanism controlling vortex shedding from rectangular bluff bodies, *Proceedings of the twelfth Australasian Fluid Mechanics Conference*, Sydney, pp.227-230, 1995.
- 12) R. Mills, J. Sheridan and K. Hourigan: Particle image velocimetry and visualization of natural and forced flow around rectangular cylinders, *Journal of Fluid Mechanics*, Vol. 478, pp.299-323, 2003.
- 13) S. Nakamura, T. Okumatsu, T. Nishikawa and T. Okabayashi: A Fatigue Damage of a Diagonal Member in a Steel Truss Bridge Due to Wind-Induced Vibration, *Developments in International Bridge Engineering - Selected Papers from Istanbul Bridge Conference*, pp.211-220, 2014.
- 14) K. Matsuda, K. Kato, K. Hisadomi and K. Harada: Low speed instability of two-dimensional rectangular prisms, *Proceedings of the ASME 2013 Pressure Vessels and Piping Conference (PVP2013)*, 97353, 2013.
- 15) T. Yagi, K. Shinjo, S. Narita, T. Nakase and H. Shirato: Interferences of vortex sheddings in galloping instability of rectangular cylinders, *Journal of Structural Engineering*, JSCE, Vol.59A, pp.552-561, 2013.(in Japanese)
- 16) Y. Nakamura and T. Mizota: Unsteady lifts and wakes of oscillating rectangular prisms, *Journal of the Engineering Mechanics Division, ASCE*, Vol.101, No.EM6, Proc. Paper 11813, pp.855-871, 1975.
- 17) K. Hirata: Study on Galloping generation mechanism. Doctor Dissertation, Kyushu University, 1993. (in Japanese)